AIP | Journal of Applied Physics

Strain effect analysis on the thermoelectric figure of merit in n-type Si/Ge nanocomposites

Y. Xu and G. Li

Citation: J. Appl. Phys. **111**, 054318 (2012); doi: 10.1063/1.3693307
View online: http://dx.doi.org/10.1063/1.3693307
View Table of Contents: http://jap.aip.org/resource/1/JAPIAU/v111/i5
Published by the American Institute of Physics.

Strain effect analysis on the thermoelectric figure of merit in *n*-type Si/Ge nanocomposites

Y. Xu and G. Li[a)]
Department of Mechanical Engineering, Clemson University, Clemson, South Carolina 29634-0921, USA

(Received 13 September 2011; accepted 11 February 2012; published online 15 March 2012)

In this paper, the effect of strain on the thermoelectric figure of merit is investigated in *n*-type Ge nanowire-Si host nanocomposite materials. The Seebeck coefficient and electrical conductivity of the Si–Ge nanocomposites are calculated using an analytical model derived from the Boltzmann transport equation (BTE) under the relaxation-time approximation. The effect of strain is incorporated into the BTE through the strain induced energy shift and effective mass variation calculated from the deformation potential theory and a degenerate $\mathbf{k} \cdot \mathbf{p}$ method at the zone-boundary *X* point. The effect of strain on the phonon thermal conductivity in the nanocomposites is computed with a model combining the strain dependent lattice dynamics and the ballistic phonon BTE. The electronic thermal conductivity is computed from the electrical conductivity using the Wiedemann-Franz law. Normal and shear strains are applied in the transverse plane of the Si–Ge nanocomposites. Thermoelectric properties, including the electrical conductivity, thermal conductivity, Seebeck coefficient, and dimensionless figure of merit, are computed for Si–Ge nanocomposites under these strain conditions.
 [http://dx.doi.org/10.1063/1.3693307]

I. INTRODUCTION

Thermoelectric materials and devices have promising applications in power generation, cooling systems, and waste heat recovery.[1–5] Driving these applications are several attractive properties of these materials, such as their being pollution-free, silent, reliable, and scalable. However, presently they are in only limited use due to their relatively low energy conversion efficiency. They are not able to match the performance of conventional refrigeration or efficiently generate power. The efficiency of thermoelectric materials is evaluated by the dimensionless figure of merit, defined as $ZT = S^2\sigma T/k_t$, in which S, σ, and T respectively denote the Seebeck coefficient, electrical conductivity, and absolute temperature and k_t represents the thermal conductivity, including contributions from phonons and electrons.[6] The key goal in thermoelectrics research is to increase ZT, but this is a challenging process because the adjustment of one parameter unavoidably involves the variation of others.[7] Recently, it has been reported that ZT values can be significantly improved in nanocomposites because of their largely increased material interfaces, which strongly scatter phonons but only slightly influence the charge carrier transport, leading to significantly reduced phonon thermal conductivity and a maintained or improved power factor $S^2\sigma$.[8,9] Compared to a state of the art thermoelectric power generation material, $Si_{0.8}Ge_{0.2}$ alloy, which has been used in space radioisotope thermoelectric power generators that operate at about 900° with a maximum efficiency of about 7%,[7] nanostructured Si–Ge bulk alloy leads to larger figures of merit as a result of decreased phonon thermal conductivity.[10,11] This method and others are being used in attempts to increase ZT values and create more universally viable thermoelectric nanocomposite materials.

Strain can be introduced into nanocomposite materials in several ways, such as phonon-induced lattice vibrations, lattice mismatch in nanocomposite growth, and applied external mechanical force. We have performed a strain analysis of the phonon thermal conductivity of $Si_{0.2}Ge_{0.8}$ nanocomposites and have found that tensile strain can significantly decrease the phonon thermal conductivity, whereas shear strain has little influence.[12] The effects of strain on electron transport in Si and Ge semiconductor devices have been extensively studied, and the results show that strain can cause a considerable change in electron mobility.[13,14] The carrier transport properties of nanostructured Si–Ge bulk alloys have been measured and analytically modeled.[10,11,15] However, to the best of our knowledge, the effect of strain on the electron transport properties of Si–Ge nanocomposites has not been investigated. In addition, the power factor and the thermal conductivity of Si and Ge respond differently to strain due to the different transport mechanisms of electrons and phonons. Because ZT is a combination of these physical quantities, how the ZT of nanocomposites will respond to external strain is in fact unknown. Investigating the effect of strain on the ZT of nanocomposites will not only help explain the behavior of nanocomposite thermoelectric materials under strain but also benefit the design and manufacturing of such materials.

In this paper, we seek to investigate the effect of mechanical deformation on the electrical transport properties and the dimensionless figure of merit of Si–Ge nanocomposite thermoelectric materials. We focus on studying the effect of externally applied stresses on the σ, S, k_t, and ZT of *n*-type $Si_{0.8}Ge_{0.2}$ nanocomposites. The strain dependent Seebeck coefficient and electrical conductivity of the Si–Ge nanocomposites are calculated using analytical models derived from the Boltzmann transport equation (BTE) under

[a)]Author to whom correspondence should be addressed. Electronic mail: gli@clemson.edu.

the relaxation-time approximation with strain induced energy shift and effective mass variation, which are computed from the deformation potential theory and using a two band degenerate $\mathbf{k}\cdot\mathbf{p}$ method. The effect of strain on the phonon thermal conductivity in the nanocomposite material is simulated based on a previously proposed model,[12] solving the ballistic phonon BTE via the finite volume method in a unit cell with phonon scattering properties calculated from strain dependent lattice dynamics. The electronic thermal conductivity is calculated from the electrical conductivity using the Wiedemann-Franz law. Then, when the strain effect models (phonon and electron) are combined, the effect of strain on the *ZT* of the nanocomposite materials is determined.

The rest of the paper is organized as follows: Sec. II describes the analytical and computational models for the calculation of the strain effect on the electron and thermal transport in $Si_{0.8}Ge_{0.2}$ nanocomposite materials and gives their strain dependent dimensionless figure of merit. Section III presents and discusses the obtained results, and Sec. IV offers conclusions.

II. THEORY

A. Strain effect on electron transport of Si–Ge nanocomposites

In order to evaluate the effect of strain on electron transport in Si–Ge nanocomposites, it is first necessary to study the band structures of Si and Ge under different strain conditions. Taking Si as an example, in unstrained *n*-type Si, electrons fill Δ valleys before Λ valleys. Generally, the Λ valleys can be ignored in electron transport simulations in Si at relatively low temperatures. In an unstrained Si crystal, there are six degenerate Δ valleys with the same minimum energy located near the *X* point at the conduction band. The distribution of electrons in these valleys can be considered as the same, given that in semiconductors such as Si and Ge, the *x*,*y*,*z* directions are equivalent in the first Brillouin zone.

However, advantageous strain reduces the symmetry of those valleys, which changes the relative population of electrons, causing subband splitting. In addition, strains along a low-symmetry axis further break crystal symmetry and result in the warping of the energy surface of subbands, leading to effective mass variation. In short, mechanical strains cause band energy splitting and warping, resulting in the variation of the conduction band minima and effective mass and leading to changes in the transport properties.

In unstrained Ge, the lowest conduction bands lie at *L* points along Λ valleys, with four degenerate valleys. However, for $Si_{1-x}Ge_x$ alloys, generally the band structure and electronic properties can be modeled as Si-like with the lowest conduction minima near the *X*-point in the Brillouin zone for $x < 0.85$ and as Ge-like with conduction band minima at the L-point for $x > 0.85$.[16] In highly strained Ge grown on $Si_{1-x}Ge_x$ with $x < 0.40$, the conduction band minimum is located in the Δ valleys.[17] Here we assume that the lowest conduction bands of $Si_{0.8}Ge_{0.2}$ nanocomposites lie at the $0.85X$ points of Δ valleys, as in Si.

The total energy of an electron in a semiconductor E_t is the sum of the carrier's potential energy E_C and the kinetic energy E.

$$E_t = E_C + E, \tag{1}$$

where E_C is the conduction band minima and E is defined by

$$E(1+\alpha E) = \frac{\hbar^2 k_l^2}{2m_l} + \frac{\hbar^2 k_{t1}^2}{2m_{t1}} + \frac{\hbar^2 k_{t2}^2}{2m_{t2}} \tag{2}$$

in the ellipsoidal coordinate system (ECS), which is usually spanned by three unit vectors $\hat{\mathbf{k}}_\mathbf{l}$, $\hat{\mathbf{k}}_\mathbf{t1}$, and $\hat{\mathbf{k}}_\mathbf{t2}$ along the principal axes of a constant-energy ellipsoid. In this dispersion equation, the nonparabolicity and anisotropicity have been accounted for to increase the accuracy, $\hbar$ is the reduced Planck's constant, and k_l/k_t are longitudinal/transverse components of the wave vector.

As discussed earlier, strain typically introduces band shift and effective mass variation. Deformation potential theory was developed to describe the energy shift introduced by strain. The energy shift of the *n*th conduction band valley due to an applied strain, ΔE_C^n, is given by[18]

$$\Delta E_C^n = \Xi_d \cdot (\varepsilon_{xx} + \varepsilon_{yy} + \varepsilon_{zz}) + \Xi_u \cdot (\hat{\mathbf{k}} \cdot \varepsilon_{ij} \cdot \hat{\mathbf{k}}), \tag{3}$$

where Ξ_d and Ξ_u are the dilation and uniaxial-shear deformation potential of the conduction band, respectively, and can be calculated from theoretical methods or fitted by experimental results. In Eq. (3), *i* and *j* represent *x*, *y*, *z*, and $\hat{\mathbf{k}}$ is the unit vector parallel to the valley *n*. Note that Eq. (3) holds for arbitrary stress/strain conditions. However, because the Δ valleys are along the [100] direction, the effect of shear strains is lost in Eq. (3). In order to account for the energy shift due to shear strain, we follow a degenerate $\mathbf{k}\cdot\mathbf{p}$ theory at the zone-boundary X point proposed by Ungersboeck *et al.*[19] Note that an *x*-*y* plane shear strain ε_{xy} shifts only the band energy of *z*-direction valleys, with[19]

$$\Delta E_{C,shear}^{\pm z} = \begin{cases} -\kappa^2 \varepsilon_{xy}^2 \Delta/4, & \kappa|\varepsilon_{xy}| < 1 \\ -(2\kappa|\varepsilon_{xy}| - 1)\Delta/4, & \kappa|\varepsilon_{xy}| > 1, \end{cases} \tag{4}$$

where Δ is the band separation between the two lowest conduction bands of the unstrained lattice at the *X* point and $\kappa = 4\Xi_p/\Delta$, with Ξ_p being the deformation potential responsible for the band splitting of the two lowest conduction bands at the zone boundary due to shear in the x-y plane.

From full band calculations, it is determined that the effect of normal stress on effective masses can be ignored, but the shear strain ε_{xy} will affect the effective masses of valleys in the *z*-direction (see Figs. 11-13 of Ref. 20). This is because the energy surface of two-fold valleys in the *z*–direction is warped due to ε_{xy} (see Fig. 14 of Ref. 20 and Fig. 2 of Ref. 21); this has been experimentally demonstrated using ultrathin-body field-effect-transistors.[20] From the same degenerate two band $\mathbf{k}\cdot\mathbf{p}$ theory, we have[19]

$$m_{l,[001]}/m_l^* = \begin{cases} (1-\kappa^2\varepsilon_{xy}^2)^{-1}, & \kappa|\varepsilon_{xy}| < 1 \\ (1-1/\kappa|\varepsilon_{xy}|)^{-1}, & \kappa|\varepsilon_{xy}| > 1, \end{cases} \quad (5)$$

$$m_{t,[110]}/m_t^* = \begin{cases} (1+\eta\kappa\varepsilon_{xy})^{-1}, & \kappa|\varepsilon_{xy}| < 1 \\ (1+\eta sgn(\varepsilon_{xy}))^{-1}, & \kappa|\varepsilon_{xy}| > 1, \end{cases} \quad (6)$$

$$m_{t,[\bar{1}10]}/m_t^* = \begin{cases} (1-\eta\kappa\varepsilon_{xy})^{-1}, & \kappa|\varepsilon_{xy}| < 1 \\ (1-\eta sgn(\varepsilon_{xy}))^{-1}, & \kappa|\varepsilon_{xy}| > 1. \end{cases} \quad (7)$$

Here, "sgn" denotes the signum function; m_l and m_t are the electron longitudinal and transverse effective masses with strain, respectively; m_l^* and m_t^* are the electron longitudinal and transverse effective masses without strain, respectively; and $\eta \approx 1 - m_t^*/m_0$ (Ref. 22), with m_0 being the free electron mass. Note that when there is no shear strain, $m_l = m_l^*$ and $m_t = m_t^*$.

In addition, the nonparabolicity coefficient in the two valleys along the z-direction is also a function of ε_{xy}; i.e.,[21]

$$\alpha^{\pm z} = \alpha_0 \frac{1+2(\eta\kappa\varepsilon_{xy})^2}{1-(\eta\kappa\varepsilon_{xy})^2}, \quad (8)$$

where α_0 is the nonparabolicity coefficient when no strain is applied, chosen as 0.5 eV^{-1} for intrinsic Si and 1.25 eV^{-1} for $Si_{0.8}Ge_{0.2}$ nanocomposites when the doping density is high.

Once again, in the current model, ε_{xy} introduces band shift, effective mass variation, and changes in the nonparabolicity coefficient of the valley pairs along the z direction only. Similarly, ε_{yz} and ε_{zx} alter band dispersion relations for valley pairs along the x and y directions, respectively.

The change in the dispersion relation changes the electron transport properties. The i-direction electrical conductivity of the nth valley σ_i^n can be calculated from an analytical model based on the BTE under the relaxation-time approximation[23]

$$\sigma_i^n = -\frac{e^2}{3}\int_0^\infty \tau^n(E)\left[v_i^n(E)\right]^2 \frac{\partial f^n(E, E_F)}{\partial E} g^n(E)dE, \quad (9)$$

where e is the electrical carrier charge, τ is the momentum relaxation time, and v_i^n is the group velocity of charge carriers in the i-direction, defined as[24]

$$v_i^n = \frac{\sqrt{2E(1+\alpha^n E)}}{\sqrt{m_i^n}(1+2\alpha^n E)}, \quad (10)$$

with m_i^n being the i-direction effective mass of the nth valley. In Eq. (9), f is the Fermi-Dirac distribution function, defined as $f = [e^{(E+E_C-E_F)/k_BT}+1]^{-1}$, where E_F is the Fermi level. For a given carrier concentration N, the Fermi level is calculated from[24]

$$N = \sum_n \int_0^\infty g^n(E) f^n(E, E_F)dE, \quad (11)$$

with $g^n(E)$ being the density of states (DOS) for the nth valley, given by[25]

$$g^n(E) = 2\sqrt{E(1+\alpha^n E)}(1+2\alpha^n E)(m_{d1}^n)^{3/2}/(\pi^2\hbar^3), \quad (12)$$

where m_{d1} is the DOS effective mass for valley n $[m_{d1}^n = (m_l m_{t1} m_{t2})^{1/3}(1+2\alpha^n E)]$.[25] Here, doped Si–Ge nanocomposites are assumed to be n-type with $N = 1e19$ cm^{-3}.

The total relaxation time is calculated by using Matthiessen's rule to combine the influences from the ionized impurity, phonon deformation potential, and grain boundary (interface) scattering mechanisms. The ionized impurity scattering rate is calculated from[26]

$$\tau_{II}^{-1} = \frac{Ne^4\mathcal{H}(1+2\alpha E)}{16\pi\sqrt{2m_{d1}}\varepsilon^2[E(1+\alpha E)]^{2/3}}, \quad (13)$$

with $\mathcal{H} = \ln(1+\gamma) - [\gamma/(1+\gamma)]$, where $\gamma = 4k^{*2}L_D^2$. Here, k^* is the effective wave vector, defined as $k^* = \sqrt{2m_{d1}E(1+\alpha E)}/\hbar$,[25] and L_D is the screening length, obtained as $L_D = [(\pi)^{2/3}\ \varepsilon^{1/2}\ \hbar]/[(3N)^{1/6}\ m_{d1}^{1/2}\ e]$.[27]

For the electron-phonon deformation potential (DP) scattering rate, we used a model proposed in Ref. 25.

$$\tau_{DP}^{-1} = \frac{\pi\ k_B T\ D_c^2\ g(E)}{\hbar\ K}\left\{\left[1-\frac{\alpha E}{1+2\alpha E}\left(1-\frac{D_v}{D_c}\right)\right]^2 - \frac{8}{3}\frac{\alpha E(1+\alpha E)}{(1+2\alpha E)^2}\frac{D_v}{D_c}\right\}. \quad (14)$$

In addition to the electron-phonon DP scattering, inter-valley optical phonon scattering can be significant. Unfortunately, inter-valley scattering parameters for single crystal silicon and germanium cannot be used to explain the experimental data for Si–Ge alloys and nanocomposites. Because of the lack of relevant experimental data for optical phonon modes, it is difficult to estimate the inter-valley scattering parameters for Si–Ge alloys and nanocomposites. In this work, we follow the approach proposed by Minnich *et al.*[15] In their approach, based on the observation that the acoustic phonon scattering and the inter-valley scattering have the same energy dependence, the effects of both scattering processes are combined in a single set of effective deformation potentials. In this work, we fit the effective deformation potentials D_c and D_v in Eq. (14) to the electrical conductivity experimental data for Si–Ge alloys and nanocomposites, with different doping densities to account for both acoustic phonon and inter-valley scattering. A detailed discussion of this issue can be found in Ref. 15.

For the grain boundary scattering rate, a model proposed in Ref. 15 is used, i.e.,

$$\tau_{GB}^{-1} = 8\pi^2 U_0^2 z_0^2 r_0^4 g(E) N_g \mathcal{I}/\hbar, \quad (15)$$

TABLE I. Parameters used to calculate electron transport properties for *n*-type Si and $Si_{1-x}Ge_x$ nanocomposites.

m_l^*/m_t^* (Ref. 17)	$0.92/0.19\ m_0$
E_d (Ref. 28)	$(1.1+3.4x)$ eV
E_u (Ref. 28)	$(10.5-0.75x)$ eV
E_p (Ref. 19)	7.0 eV
Δ (Ref. 19)	0.53 eV
Low frequency permittivity (Ref. 16)	$\varepsilon=(11.7+4.5x)\varepsilon_0$[a]
Electron/hole deformation potential (heavily doped $Si_{1-x}Ge_x$)	$D_c=12.5$ eV, $D_v=5.0$ eV (Ref. 29)
Electron/hole deformation potential (intrinsic Si)	$D_c=9.0$ eV(Ref. 30), $D_v=5.0$ eV(Ref. 29)
Bulk modulus (Ref. 16)	$K=(97.9-22.8x)$ GPa
Grain boundary potential parameters (Ref. 15)	$U_0=45$ meV, $z_0=2.0$ nm, $r_0=1.0$ nm

[a]ε_0= vacuum permittivity.

with the number density of the interface $N_g=4\,L_{Ge}/(\pi\,r_0^2\,L_{Si}^2)$ and with $\mathcal{I}$ given by Eq. (22) in Ref. 15. Other parameters can be found in Table I. For $Si_{1-x}Ge_x$ alloy and nanocomposites, effective properties such as the bulk modulus K, the low frequency permittivity ε, and the deformation potentials E_d and E_u are calculated as functions of x from a first order (linear) interpolation.[16] For E_p, the value of Si is used.

The total electrical conductivity is obtained by summing the contributions of electrons from all six valleys.[31] Because these valleys are differently oriented, it is convenient to introduce a reference coordinate system defining some general directions. Here the crystal coordinate system (CCS) is chosen; it consists of the lattice basis vectors $\hat{\mathbf{k}}_\mathbf{1}$, $\hat{\mathbf{k}}_\mathbf{2}$, and $\hat{\mathbf{k}}_\mathbf{3}$, oriented along the three orthogonal [100] crystallographic directions of the underlying material. The CCS and the ECS are related in the reciprocal space. The direct relation between them depends on the material under consideration. For a given conduction band ellipsoid in a given material, the unit basis vectors $\hat{\mathbf{k}}_\mathbf{l}$, $\hat{\mathbf{k}}_\mathbf{t1}$, and $\hat{\mathbf{k}}_\mathbf{t2}$ in the ECS can be expressed in the CCS, forming a rotation matrix $\Re_{E\leftarrow C}$, which defines the direction cosine of the principal axes of this ellipsoid with respect to the coordinates of the CCS. Different ellipsoid transformation matrices in the unstrained case are shown in Ref. 32 for sixfold-degenerate Δ and eightfold-degenerate Λ valleys. For Si, there are six degenerate constant energy Δ valley conduction band ellipsoids, as shown in Fig. 1. The basis vectors are unique for each ellipsoid in the ECS, with $\hat{\mathbf{k}}_\mathbf{l}$ along the major axis and $\hat{\mathbf{k}}_\mathbf{t1}$ and $\hat{\mathbf{k}}_\mathbf{t2}$ perpendicular to it. There is a unique transformation matrix $\Re_{E\leftarrow C}$ for each ellipsoid, with the rows coming from the components of $\hat{\mathbf{k}}_\mathbf{l}$, $\hat{\mathbf{k}}_\mathbf{t1}$, and $\hat{\mathbf{k}}_\mathbf{t2}$. For instance, for ellipsoid 1 in Fig. 1, $\hat{\mathbf{k}}_\mathbf{l}=(1\,0\,0)$, $\hat{\mathbf{k}}_\mathbf{t1}=(0\,1\,0)$, and $\hat{\mathbf{k}}_\mathbf{t2}=(0\,0\,1)$; thus,

$$\Re_{E\leftarrow C}^{\Delta_1}=\begin{bmatrix}1&0&0\\0&1&0\\0&0&1\end{bmatrix}. \tag{16}$$

The transformation matrices for other ellipsoids can be obtained similarly. In all our simulations, the CCS is fixed in real space, and the ECS depends on the specific material and is unique to each ellipsoid.

When strains are applied, the wave vectors between deformed and undeformed crystal configurations is related by $\mathbf{F}^{-T}$, with $\mathbf{F}$ being the deformation gradient tensor. Accordingly, after deformation, the directional cosines matrix C becomes $C=\mathbf{F}^{-T}\Re_{E\leftarrow C}^{-1}$.

The total conductivity is then calculated as

$$\sigma_{ij}=\sum_n^6\sum_p^3 c_{ip}^n\sigma_p^n[c_{pj}^n]^{-1}, \tag{17}$$

in which c_{ip}^n and $[c_{pj}^n]^{-1}$ are components of the nth directional cosine matrix C^n and its inverse matrix.

The Seebeck coefficient is then calculated by

$$S_{ij}=\frac{\sum_n^6\sum_p^3 c_{ip}^n S_p^n\sigma_p^n[c_{pj}^n]^{-1}}{\sigma_{ij}}, \tag{18}$$

with

$$S_i^n=-\frac{1}{eT}\frac{\int_0^\infty\tau^n(E)[v_i^n(E)]^2[\partial f^n(E,E_F)/\partial E](E-E_F)g^n(E)dE}{\int_0^\infty\tau^n(E)[v_i^n(E)]^2[\partial f^n(E,E_F)/\partial E]g^n(E)dE}. \tag{19}$$

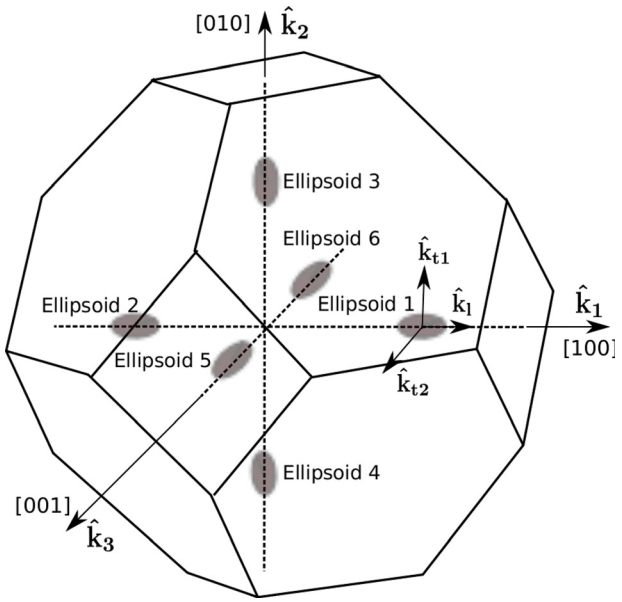

FIG. 1. (Color online) Conduction band constant energy ellipsoids along Δ for Si.

Note that although phonon drag effects can be large at low temperatures in silicon (around 1/5 of the Debye temperature), they are generally reduced by alloying and increasing temperature.[33] For the temperature range we consider in this work (300 K to 800 K), phonon-drag effects are not included in the calculations.

B. Strain effect on thermal transport of Si–Ge nanocomposites

In order to examine the effects of strain on the phonon thermal transport of Si–Ge nanocomposites, we have developed a model based on phonon BTE with strain dependent thermodynamic and phonon scattering properties calculated from lattice dynamics. This model is described in detail in Ref. 12; a short summary is given below.

Tersoff empirical interatomic potentials are used to describe the atomic interactions in Si and Ge lattices. Mechanical strains are related to crystal lattice deformation by the Cauchy-Born rule. For a deformed crystal lattice, the lattice dynamics theory is employed to derive the strain-dependent dynamical matrix $\mathbf{D}(\mathbf{k})$ for wave vector $\mathbf{k}$ in the deformed configuration of the first Brillouin zone; i.e.,[34]

$$\mathbf{D}(\mathbf{k}) = \frac{1}{M}\begin{bmatrix} \sum_{\kappa} \bar{\Phi}^{11}_{j,k}(\iota,\kappa) e^{i\mathbf{k}^0\cdot\left(\mathbf{X}^0_\kappa - \mathbf{X}^0_\iota\right)} & \sum_{\kappa} \bar{\Phi}^{12}_{j,k}(\iota,\kappa) e^{i\mathbf{k}^0\cdot\left(\mathbf{X}^0_\kappa - \mathbf{X}^0_\iota - \mathbf{F}^{-1}\xi\right)} \\ \sum_{\kappa} \bar{\Phi}^{21}_{j,k}(\iota,\kappa) e^{i\mathbf{k}^0\cdot\left(\mathbf{X}^0_\kappa - \mathbf{X}^0_\iota + \mathbf{F}^{-1}\xi\right)} & \sum_{\kappa} \bar{\Phi}^{22}_{j,k}(\iota,\kappa) e^{i\mathbf{k}^0\cdot\left(\mathbf{X}^0_\kappa - \mathbf{X}^0_\iota\right)} \end{bmatrix}, \tag{20}$$
$$\iota = 1, \quad j,k = 1,2,3, \quad \iota \in B_p, \quad \kappa \in B_q, \quad p,q = 1,2,$$

where M is the atomic mass; $\bar{\Phi}^{pq}_{j,k}(\iota,\kappa)$ denotes the force constant between the jth component of atom ι in Bravais lattice p (B_p) and the kth component of atom κ in Bravais lattice q (B_q); $\mathbf{k}^0$ represents the corresponding wave vector in the undeformed crystal lattice; $\mathbf{X}^0_\iota$ and $\mathbf{X}^0_\kappa$ are the equilibrium positions of atoms ι and κ in the undeformed crystals, respectively; $\boldsymbol{\xi}$ denotes the inner displacement of the two fcc Bravais lattices and is calculated by minimizing the Helmholtz free energy of the lattice; and $\mathbf{F}^{-1}$ is the inverse tensor of the deformation gradient $\mathbf{F}$ of the two Bravais lattices. The phonon frequencies of the strained bulk Si and Ge are then calculated by taking the square root of the eigenvalues of the abovementioned strain dependent dynamical matrix.

For a given $\mathbf{F}$, the calculated phonon frequency spectrum of Si and Ge lattices is used to compute the bulk thermodynamic properties of Si and Ge, including the phonon specific heat, group velocity, and phonon mean free path. The phonon specific heat for the sth polarization of wavevector $\mathbf{k}$ is determined by

$$C_{s\mathbf{k}} = k_B \frac{\left(\frac{\hbar\omega_{s\mathbf{k}}}{k_B T}\right)^2 e^{\hbar\omega_{s\mathbf{k}}/k_B T}}{\left(e^{\hbar\omega_{s\mathbf{k}}/k_B T} - 1\right)^2}, \tag{21}$$

where $\omega_{s\mathbf{k}}$ is the corresponding frequency. The average phonon specific heat is obtained by summing $C_{s\mathbf{k}}$ over the acoustic branches.

$$C = \sum_{\mathbf{k}} \sum_{s=1}^{3} C_{s\mathbf{k}}, \quad s \in \text{acoustic phonon branches}. \tag{22}$$

The acoustic phonon group velocity for the sth polarization of wavevector $\mathbf{k}$ is calculated by

$$v_{s\mathbf{k}} = \left|\frac{\partial\omega_{s\mathbf{k}}}{\partial\mathbf{k}}\right|. \tag{23}$$

Then the average phonon group velocity can be obtained as

$$v = \frac{\sum_{\mathbf{k}} \sum_{s=1}^{3} C_{s\mathbf{k}} v_{s\mathbf{k}}}{C}, \quad s \in \text{acoustic phonon branches}. \tag{24}$$

The average phonon mean free path (MFP) is computed from approximated kinetic theory by[35]

$$\Lambda \approx \frac{3k_b}{Cv}, \tag{25}$$

with the bulk thermal conductivity k_b calculated via the Slack relation.[36]

In Eqs. (22), (24), and (25), only the acoustic branches of the phonon dispersion are included for a better approximation of the average phonon MFP, as optical phonons contribute little to the thermal conductivity for Si and Ge due to their small group velocities in the temperature range we considered.[35,37] Note that because the phonon frequencies $\omega_{s\mathbf{k}}(\mathbf{F}, \boldsymbol{\xi})$ depend on the applied strain, thermodynamic properties such as C, v, Λ, and k_b are all functions of strain. For the simplicity of notation, "$(\mathbf{F}, \boldsymbol{\xi})$" is not shown explicitly in their equations.

These properties are then used in a "gray" BTE to calculate the effective phonon thermal conductivity of the Si–Ge nanocomposites.

$$\nabla \cdot (I(\mathbf{r}, \mathbf{s}) \cdot \mathbf{s}) = -\frac{I(\mathbf{r}, \mathbf{s}) - I_0(\mathbf{r})}{\Lambda}, \tag{26}$$

where $I(\mathbf{r}, \mathbf{s})$ represents the phonon intensity at a spatial position $\mathbf{r}$ over a path length ds in the direction of the unit vector $\mathbf{s}$, and $I_0(\mathbf{r})$ denotes the equivalent equilibrium phonon intensity.

For a given nanocomposite material, the phonon intensity $I(\mathbf{r}, \mathbf{s})$ is obtained by solving Eq. (26) numerically. In this work, we consider $Si_{1-x}Ge_x$ with Ge nanowires

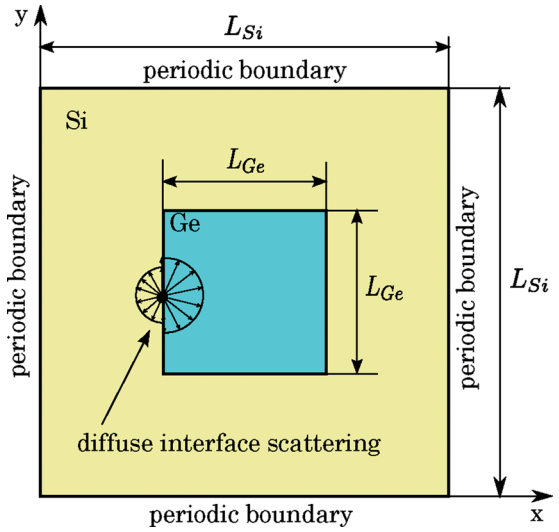

FIG. 2. (Color online) Unit cell of $Si_{1-x}Ge_x$ nanocomposite for numerical solution of the BTE and calculation of the phonon thermal conductivity of the materials.

embedded in a Si matrix. The Ge nanowires are uniformly distributed in parallel, and strains are applied in the transverse plane. In this case, the BTE can be solved to obtain the phonon intensity by using the finite volume method in a 2D unit cell of the nanocomposites with periodic boundary conditions and a diffuse mismatch interface model, as shown in Fig. 2, with the edge length of the unit cell L_{Si} and the edge length of a Ge nanowire L_{Ge}. For the top $(y = L_{Si})$ and bottom $(y = 0)$ edges, the periodic boundary condition implies that phonons coming in equal phonons going out for all x and $\mathbf{s}$; i.e.,

$$I(x, L_{Si}, \mathbf{s}) = I(x, 0, \mathbf{s}). \tag{27}$$

For the right $(x = 0)$ and left $(x = L_{Si})$ edges, the periodic boundary condition means that the deviation between the phonon intensities in any given direction at the right and left edges is independent of y; i.e.,

$$I(0, y, \mathbf{s}) - I(L_{Si}, y, \mathbf{s}) = \frac{v_{Si}C_{Si}\Delta T}{4\pi}, \tag{28}$$

where v_{Si} and C_{Si} represent the average group velocity and acoustic specific heat of Si, respectively, and ΔT denotes the temperature difference. The diffuse interface scattering assumes that at the interface, part of the phonons are transmitted through while the rest are reflected back and are evenly distributed across all angles on each side of the interface.

After the phonon intensities are obtained, the effective phonon thermal conductivity of Si–Ge nanocomposites k_p is calculated using Fourier's law.

$$k_p = \frac{\int_0^{L_{Si}} q_x(x, y)\mathrm{d}y}{\bar{T}(0) - \bar{T}(L_{Si})}, \tag{29}$$

where q_x is the heat flux in the x-direction and $\bar{T}(0)$ and $\bar{T}(L_{Si})$ are the average temperatures at $x = 0$ and $x = L_{Si}$, respectively. More details can be found in Ref. 12.

The electronic thermal conductivity k_e is calculated via the Wiedemann-Franz law as $k_e = L_z\sigma T$, where L_z is the Lorenz number. Here we assume that the nanocomposites are heavily doped, and L_z for metals is used.

C. Strain effect on figure of merit of Si–Ge nanocomposites

Once the strain dependent phonon thermal conductivity and electrical properties have been obtained, the calculation of the dimensionless figure of merit of nanocomposite thermoelectric materials is straightforward; i.e., $ZT = S^2\sigma T/(k_p + k_e)$.

III. RESULTS AND DISCUSSION

A. Thermoelectric properties of $Si_{0.8}Ge_{0.2}$ nanocomposites

This section investigates the effect of strain on the electrical properties of bulk Si and $Si_{1-x}Ge_x$ nanocomposites. To validate the electrical conductivity model described in Sec. II A, we calculated the electrical conductivities of unstrained $Si_{0.7}Ge_{0.3}$ alloys and $Si_{0.8}Ge_{0.2}$ nanocomposites with different doping densities and compared them with available experimental data obtained from Refs. 15, 33, and 38, as shown in Fig. 3. The computational results show good agreement with the experimental data.

The effect of strain on electrical conductivity is verified by comparison of the electron mobility of intrinsic Si for [100] uniaxial strain with data from Ungersboeck *et al.*'s work,[19] as shown in Fig. 4. The results show a similar dependence on strain as in Ungersboeck's results, although they are not exactly the same. The difference comes from the different modeling approaches and different scattering mechanisms considered. Our results are based on an analytical model derived from the BTE with several fitting parameters. The results in Ref. 19 were calculated numerically by solving the semiclassical BTE using a Monte Carlo method. We considered ionized impurity and phonon deformation

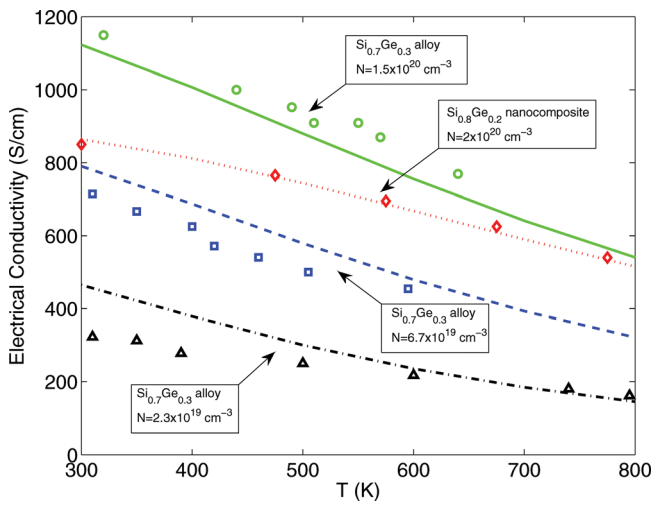

FIG. 3. (Color online) Experimental (symbols) and computed (curves) electrical conductivity of $Si_{70}Ge_{30}$ alloy and $Si_{0.8}Ge_{0.2}$ nanocomposite as a function of temperature.

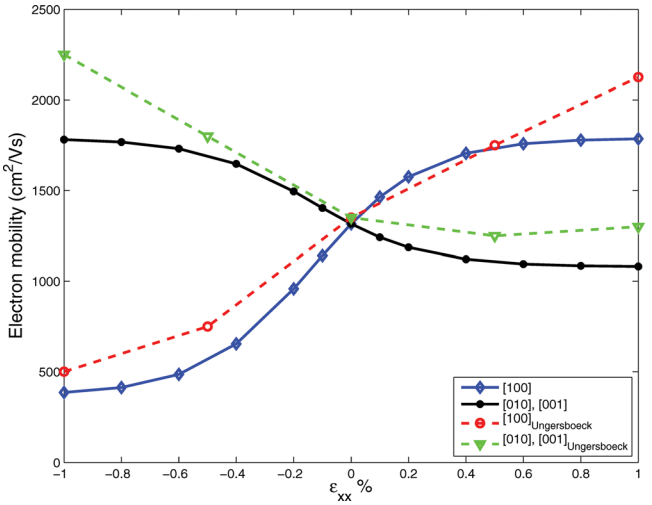

FIG. 4. (Color online) Bulk electron mobility of intrinsic Si as a function of strain for stress along the [100] direction.

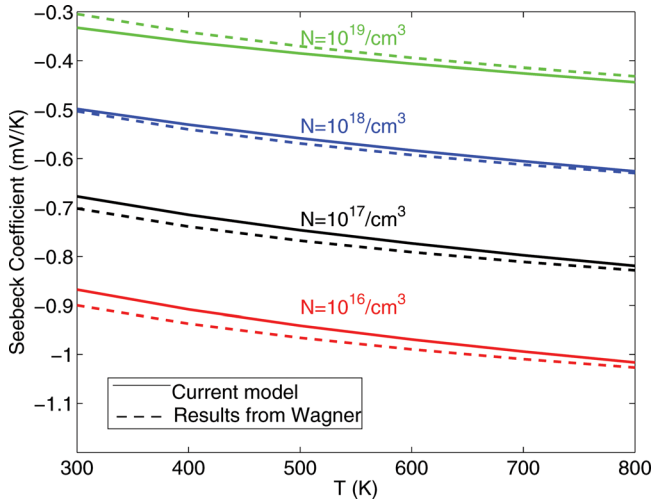

FIG. 6. (Color online) Temperature and doping dependence of Seebeck coefficient of Si. Solid curves: results from current model. Dashed curves: results from Wagner (Ref. 39).

potential scatterings, whereas Ungersboeck's models contained ionized impurity scattering, phonon scattering, alloy scattering, and impact ionization scattering. Figure 5 shows the electron mobility enhancement of intrinsic Si as a function of strain for the stress direction along [100] calculated from our model and experimental results obtained from Ref. 20. Our results show trends similar to those of the experimental data. From the two figures, we observe that uniaxial tensile strain along the [100] direction increases electron mobility in the same direction but decreases it in the two perpendicular directions, which implies a possible change in the thermoelectric power factor.

The Seebeck coefficient of unstrained bulk Si with a doping density of $10^{16}/\text{cm}^3$ to $10^{19}/\text{cm}^3$ is shown in Fig. 6. The solid lines represent the Seebeck coefficients calculated from our model, and the dashed lines are from Fig. 3.8 of Ref. 39. The results indicate that the Seebeck coefficient decreases with increasing temperature, and further decreases with decreasing doping density.

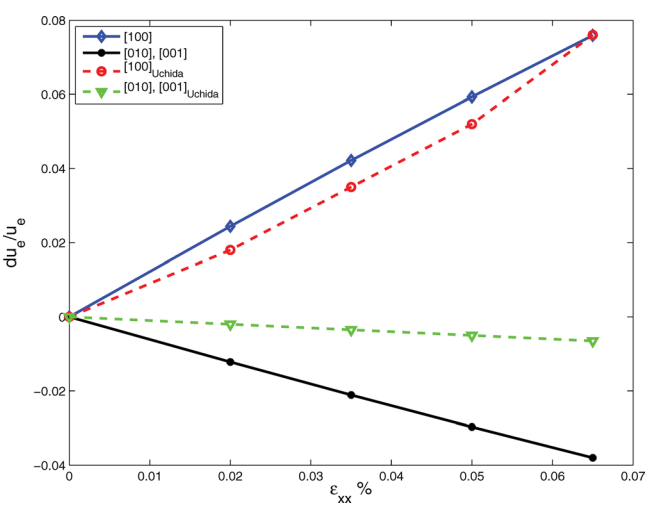

FIG. 5. (Color online) Electron mobility enhancement of intrinsic Si as a function of strain for stress along the [100] direction.

B. Strain effect on figure of merit of $Si_{0.8}Ge_{0.2}$ nanocomposites

Three types of stresses are applied in the transverse plane (assumed to be the (001) plane) of the $Si_{0.8}Ge_{0.2}$ nanocomposites in order to study the effect of strain on their thermoelectric properties. As shown in Fig. 7, the applied stresses are (1) uniaxial stress in the [100] direction, (2) uniaxial stress in the [110] direction, and (3) biaxial stress in the [100] and [010] directions. These stresses are applied such that the resultant strains are, respectively, (1) 1% normal strain in the [100] direction, (2) a shear strain of 0.01 on the (001) plane, and (3) 1% biaxial normal strain in the [100] and [010] directions. In addition, to show the effect of the size of the Ge nanowires, $L_{Ge} = 10\text{nm}$ and $L_{Ge} = 20\text{nm}$ are used in the calculations, with the atomic percentage of Si and Ge remaining fixed. The doping density of the $Si_{0.8}Ge_{0.2}$ nanocomposites is set at $N = 10^{19}\ \text{cm}^{-3}$.

The calculated Seebeck coefficient, electrical conductivity, phonon thermal conductivity, and figure of merit are shown in Figs. 8–10 for $L_{Ge} = 10\text{nm}$ and Figs. 11–13 for $L_{Ge} = 20\text{nm}$. For the two nanowire sizes, as shown in Figs. 8 and 11, the tensile strain along the [100] direction increases the electrical conductivity and the Seebeck coefficient and at the same time decreases the thermal conductivity along the direction in which the stress is applied, resulting in an increase in the dimensionless figure of merit along the applied stress

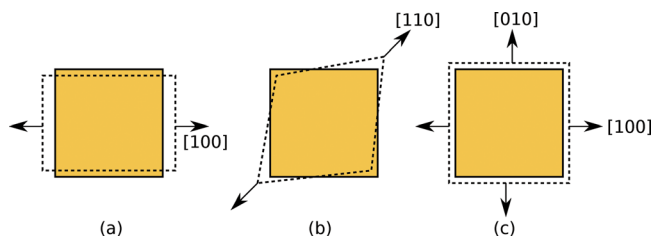

FIG. 7. (Color online) Three types of stresses applied on the $Si_{0.8}Ge_{0.2}$ nanocomposites: (a) uniaxial stress in the [100] direction, (b) uniaxial stress in the [110] direction producing a shear strain on the (001) plane, and (c) biaxial stress in the [100] and [010] directions.

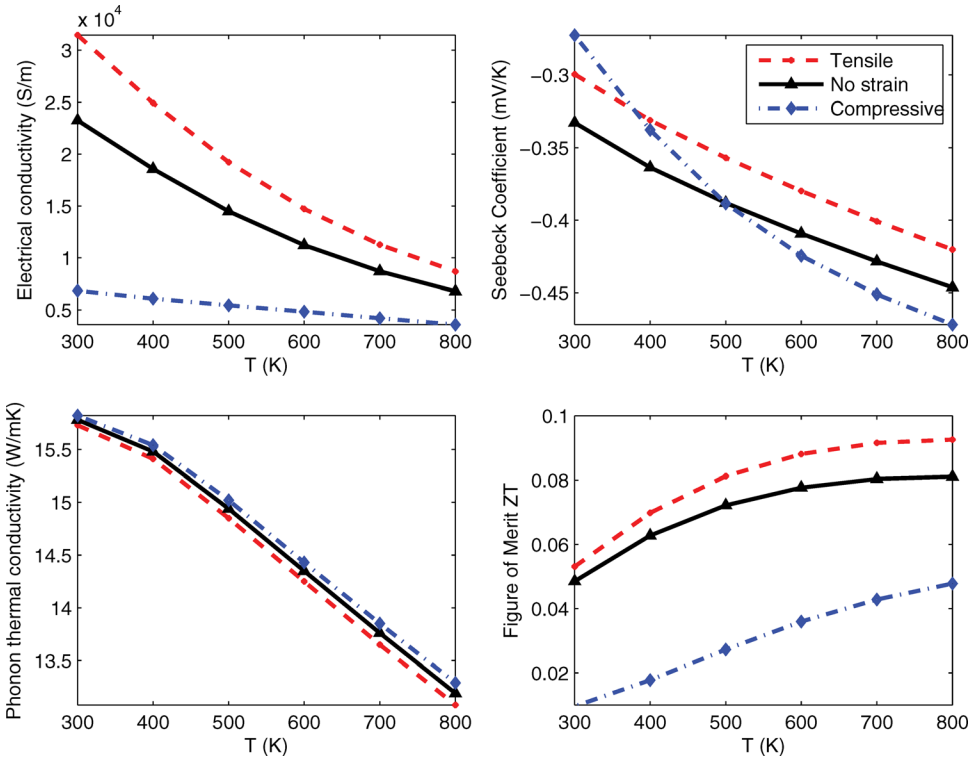

FIG. 8. (Color online) Thermoelectric properties of $Si_{0.8}Ge_{0.2}$ with $N = 10^{19}$ cm^{-3} under 1% normal strain in the [100] direction when $L_{Ge} = 10$ nm.

direction. The compressive strain in the [100] direction largely decreases the electrical conductivity and, at the same time, increases the phonon thermal conductivity. Under the compressive strain in the [100] direction, the rate of decrease of the Seebeck coefficient with increasing temperature is higher than that in the tensile strain case. Even though the magnitude of the Seebeck coefficient increases with compressive strain at higher temperatures, ZT still decreases under compressive strain in the [100] direction. Figures 9 and 12 show that the shear strain due to the applied stresses along the [110] direction largely decreases the electrical conductivity and increases the Seebeck coefficient in the [100] direction for both tension and compression loads. Note that in *n*-type semiconductors, the Seebeck coefficients are negative. The resultant power factor is decreased by the shear strain. At the same time, tension/compression loads in the [110] direction decrease/increase the phonon thermal conductivity in the [100] direction. Due to the combined effect, the shear strain

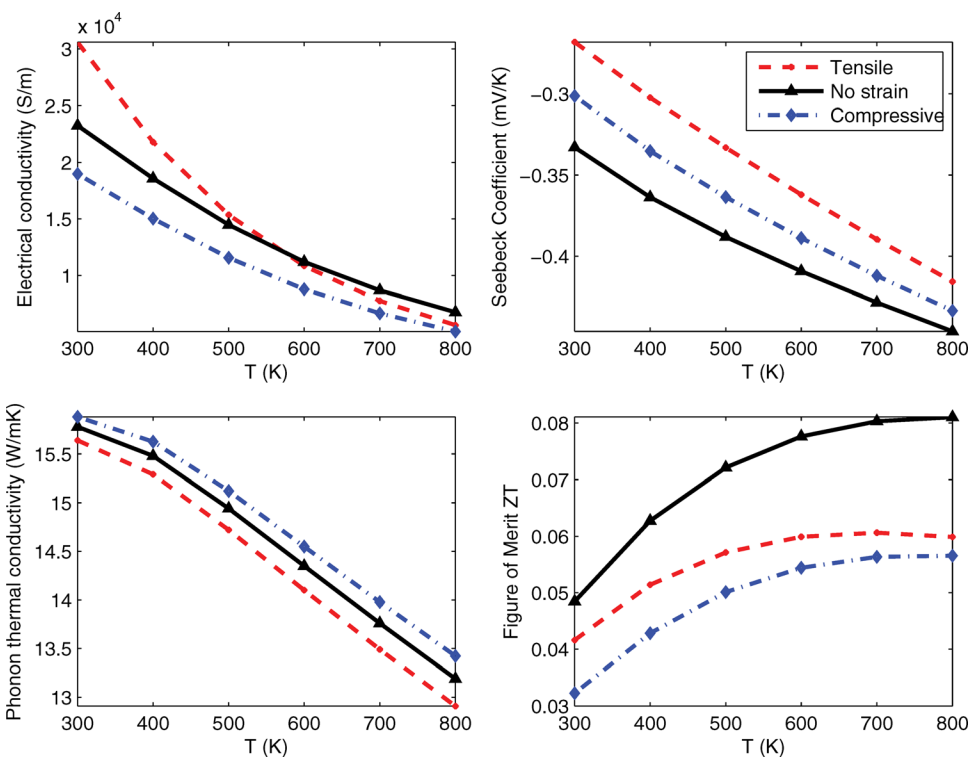

FIG. 9. (Color online) Thermoelectric properties of $Si_{0.8}Ge_{0.2}$ with $N = 10^{19}$ cm^{-3} under a shear strain of 0.01 $L_{Ge} = 10$ nm.

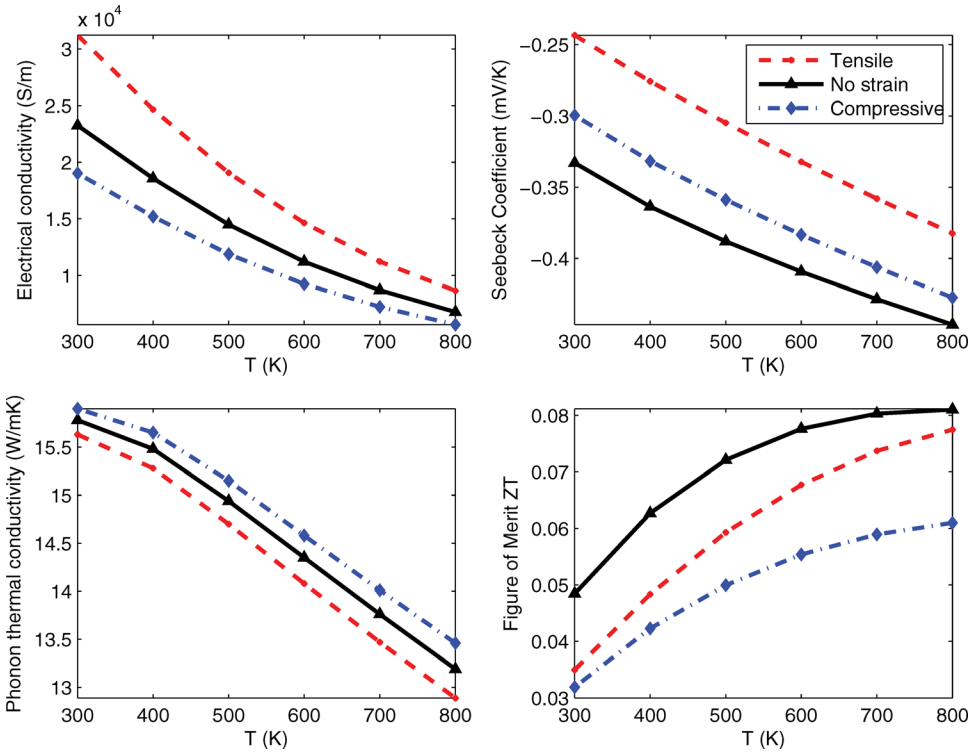

FIG. 10. (Color online) Thermoelectric properties of $Si_{0.8}Ge_{0.2}$ with $N = 10^{19}$ cm^{-3} under 1% biaxial strain when $L_{Ge} = 10$ nm.

leads to a drop in ZT in the [100] direction. Figures 10 and 13 show the effect of strain on the thermoelectric properties of $Si_{0.8}Ge_{0.2}$ nanocomposites along the [100] and [010] directions in which biaxial normal strain occurs. The results indicate that biaxial tensile strain increases the electrical conductivity and the Seebeck coefficient, whereas biaxial compressive strain decreases the electrical conductivity but increases the Seebeck coefficient. The phonon thermal conductivity is decreased by tensile strain and increased by compressive strain. When these effects are combined, we observed that the ZT decreases under biaxial normal strain.

If we compare the figures of merit under different strains, the uniaxial tensile strain is the only case that leads to an increase in the figure of merit. This increase becomes clearer when the temperature increases. At 800 K, 1% uniaxial tensile strain results in a 15% increase of the dimensionless figure of merit in $Si_{0.8}Ge_{0.2}$ nanocomposites. The corresponding dimensionless figure of merit is 0.093.

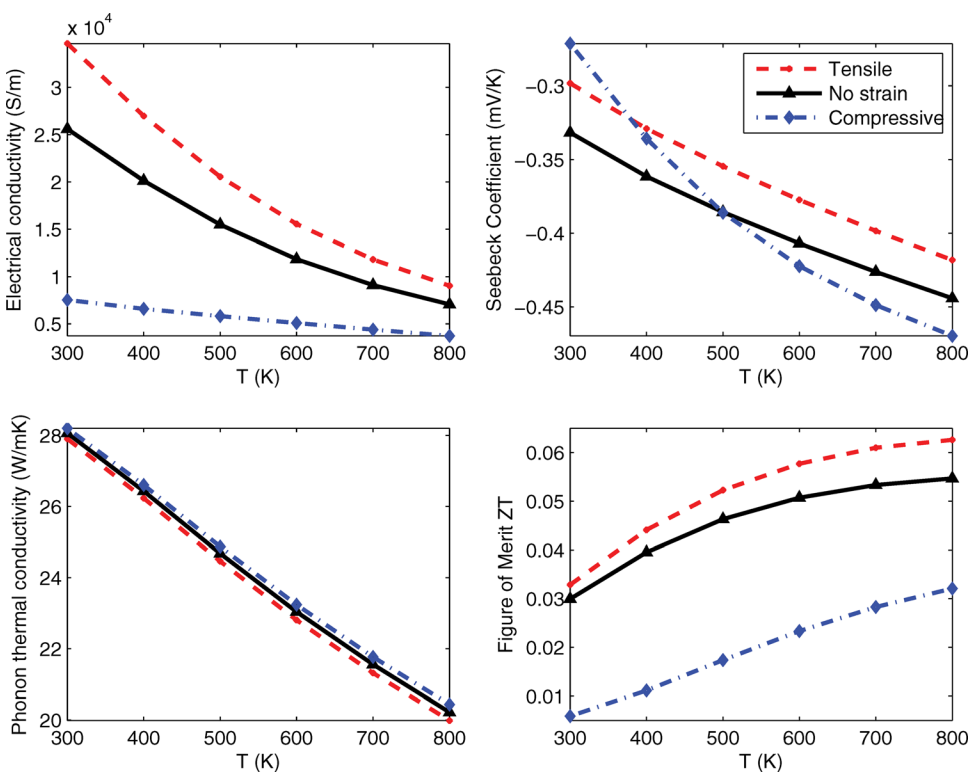

FIG. 11. (Color online) Thermoelectric properties of $Si_{0.8}Ge_{0.2}$ with $N = 10^{19}$ cm^{-3} under 1% normal strain in the [100] direction when $L_{Ge} = 20$ nm.

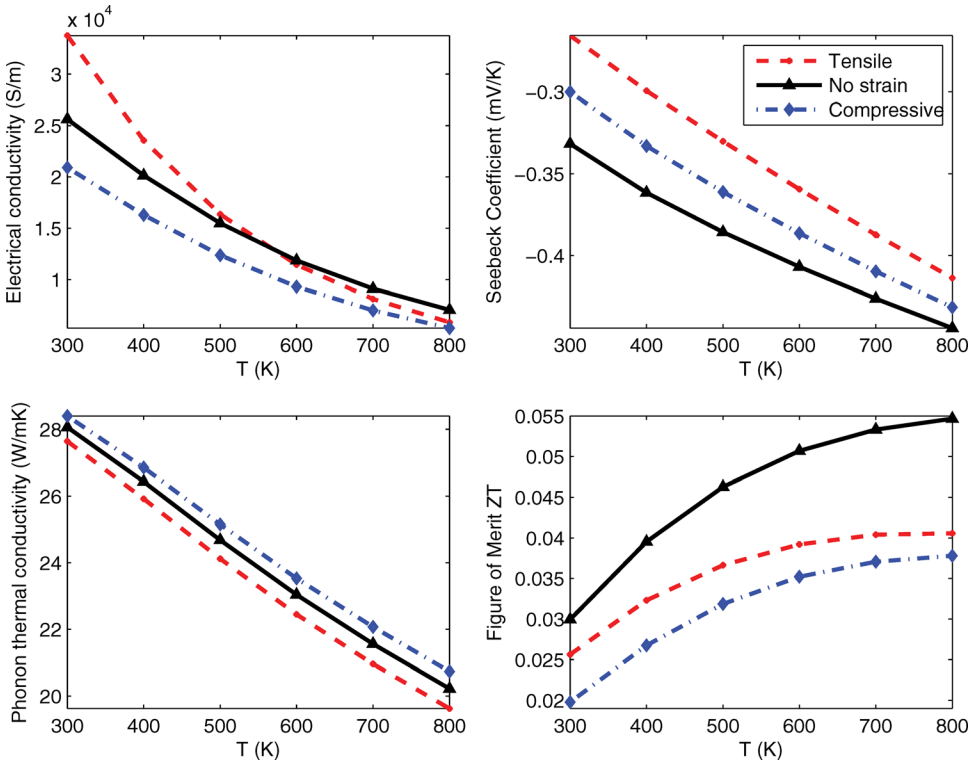

FIG. 12. (Color online) Thermoelectric properties of $Si_{0.8}Ge_{0.2}$ with $N = 10^{19}$ cm^{-3} under a shear strain of 0.01 when $L_{Ge} = 20$ nm.

When we compare the results for the two Ge nanowire sizes, $L_{Ge} = 10$ nm and $L_{Ge} = 20$ nm, we observe that the decrease in the Ge nanowire size causes a greater reduction of the phonon thermal conductivity than of the electrical conductivity, leading to a higher ZT. Considering Figs. 8 and 11, for example, when L_{Ge} decreases from 20 nm to 10 nm, the phonon thermal conductivity decreases by about 40%, but the electrical conductivity decreases by less than 10%. This behavior is due to the stronger phonon scattering at Si–Ge interfaces when the characteristic length of the material components decreases, as many authors have pointed out in the literature.[8–11] In addition, our results show that the strain effect on the thermoelectric properties is similar for the two Ge nanowire sizes, which implies that the strain effect is insensitive to the characteristic length of the material components.

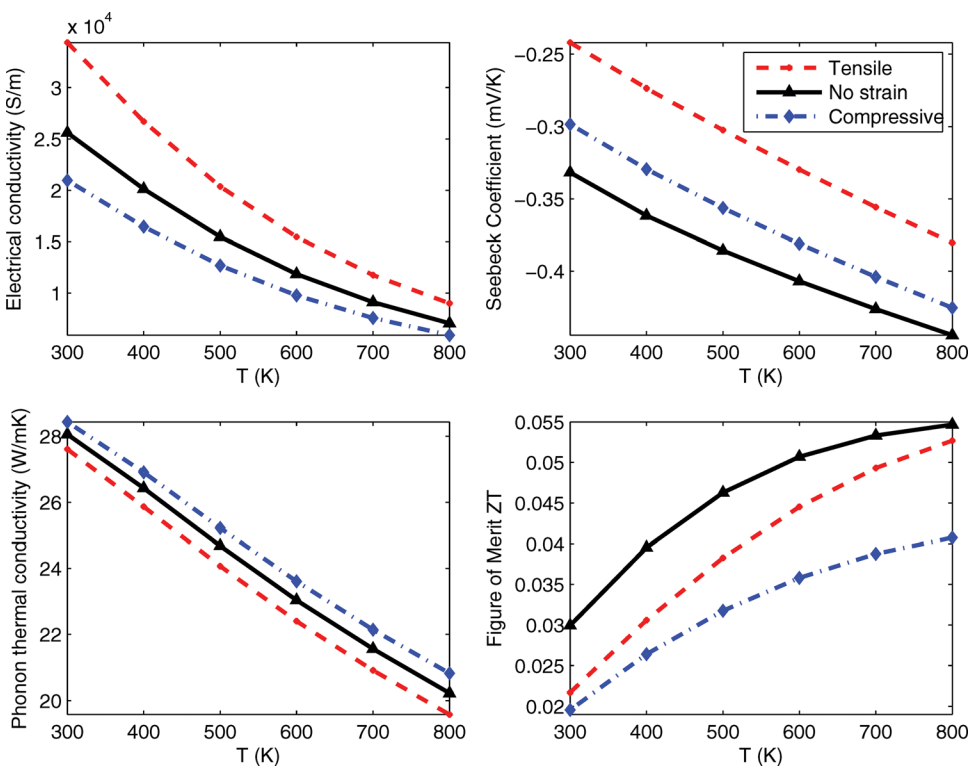

FIG. 13. (Color online) Thermoelectric properties of $Si_{0.8}Ge_{0.2}$ with $N = 10^{19}$ cm^{-3} under 1% biaxial strain when $L_{Ge} = 20$ nm.

IV. CONCLUSION

The effect of strain on the thermoelectric properties of Si–Ge nanocomposites is investigated in this paper. The effect of strain on electron transport was studied via the use of an analytical model derived from the BTE with band structures obtained from a degenerate $\mathbf{k} \cdot \mathbf{p}$ theory. The effect of strain on thermal transport was studied by solving the phonon BTE using strain dependent phonon scattering properties calculated from lattice dynamics. Our results confirm that nanocomposites are better thermoelectric materials than their alloys. In the 300-800 K temperature range, uniaxial tensile strain along the [100] direction can improve the ZT parallel to the tension direction. Compressive strain in the [100] direction, biaxial strain along the [100] and [010] directions, and uniaxial stress along [110] decrease ZT. At 800 K with a doping density of 10^{19}cm^{-3}, 1% uniaxial tensile strain along the [100] direction can increase the figure of merit of $Si_{0.8}Ge_{0.2}$ nanocomposites by 15% to $ZT = 0.093$.

ACKNOWLEDGMENTS

We gratefully acknowledge support from the National Science Foundation under Grant Nos. CMMI-0800474 and CBET-0955096 and from the Clemson University start-up funds.

[1]W. A. Wong, D. J. Anderson, K. L. Tuttle, and R. C. Tew, AIP Conf. Proc. **813**(1), 340 (2006).
[2]E. F. Thacher, B. T. Helenbrook, M. A. Karri, and C. J. Richter, Proc. Inst. Mech. Eng., Part D (J. Automob. Eng.) **221**, 95 (2007).
[3]G. Mahan, B. Sales, and J. Sharp, Phys. Today **50**(3), 42 (1997).
[4]F. J. DiSalvo, Science **285**(5428), 703 (1999).
[5]L. E. Bell, Science **321**(5895), 1457 (2008).
[6]H. J. Goldsmid, *Thermoelectric Refrigeration* (Plenum, New York, 1964).
[7]G. Chen, M. S. Dresselhaus, G. Dresselhaus, J.-P. Fleurial, and T. Caillat, Int. Mater. Rev. **48**(1), 45 (2003).
[8]R. Venkatasubramanian, E. Siivola, T. Colpitts, and B. O'Quinn, Nature **413**(6856), 597 (2001).
[9]B. Zhang, J. He, X. Ji, T. M. Tritt, and A. Kumbhar, Appl. Phys. Lett. **89**(16), 163114 (2006).
[10]G. Joshi, H. Lee, Y. Lan, X. Wang, G. Zhu, D. Wang, R. W. Gould, D. C. Cuff, M. Y. Tang, M. S. Dresselhaus, G. Chen, and Z. Ren, Nano Lett. **8**(12), 4670 (2008).
[11]X. W. Wang, H. Lee, Y. C. Lan, G. H. Zhu, G. Joshi, D. Z. Wang, J. Yang, A. J. Muto, M. Y. Tang, J. Klatsky, S. Song, M. S. Dresselhaus, G. Chen, and Z. F. Ren, Appl. Phys. Lett. **93**(19), 193121 (2008).
[12]Y. Xu and G. Li, J. Appl. Phys. **106**(11), 114302 (2009).
[13]M. Chu, Y. Sun, U. Aghoram, and S. E. Thompson, Annu. Rev. Mater. Res. **39**(1), 203 (2009).
[14]Y. Sun, S. E. Thompson, and T. Nishida, *Strain Effect in Semiconductors: Theory and Device Applications* (Springer, New York, 2010).
[15]A. J. Minnich, H. Lee, X. W. Wang, G. Joshi, M. S. Dresselhaus, Z. F. Ren, G. Chen, and D. Vashaee, Phys. Rev. B **80**(15), 155327 (2009).
[16]*Properties of Advanced Semiconductor Materials: GaN, AlN, InN, BN, SiC, SiGe*, edited by M. E. Levinshtein, S. L. Rumyantsev, and M. S. Shur (John Wiley & Sons, New York, 2001), Chap. 6, pp. 149–187.
[17]M. M. Rieger and P. Vogl, Phys. Rev. B **48**, 14276 (1993).
[18]I. Balslev, Phys. Rev. **143**(2), 636 (1966).
[19]E. Ungersboeck, S. Dhar, G. Karlowatz, V. Sverdlov, H. Kosina, and S. Selberherr, IEEE Trans. Electron Devices **54**, 2183 (2007).
[20]K. Uchida, T. Krishnamohan, K. C. Saraswat, and Y. Nishi, in Proceedings of the 2005 IEEE International Electron Devices Meeting, Washington, DC, 5 December 2005, pp. 129–132.
[21]V. Sverdlov, E. Ungersboeck, H. Kosina, and S. Selberherr, in Proceedings of the 2007 IEEE 37th European Solid State Device Research Conference, Munich, Germany, 11–13 September 2007, pp. 386–389.
[22]V. Sverdlov, T. Windbacher, and S. Selberherr, in Proceedings of the 2008 International Conference on Simulation of Semiconductor Processes and Devices, Hakone, Japan, 9–11 September 2008, pp. 145–148.
[23]G. Chen, *Nanoscale Energy Transport and Conversion: A Parallel Treatment of Electrons, Molecules, Phonons, and Photons* (Oxford University Press, New York, 2005).
[24]A. Minnich, "Modeling the Thermoelectric Properties of Bulk and Nanocomposite Thermoelectric Materials," M.S. thesis, Massachusetts Institute of Technology, 2008.
[25]Y. I. Ravich, B. A. Efimova, and V. I. Tamarchenko, Phys. Status Solidi B **43**, 11 (1971).
[26]M. Lundstrom, *Fundamentals of Carrier Transport* (Cambridge University Press, Cambridge, England, 2000).
[27]W. Zawadzki and W. Szymańska, Phys. Status Solidi B **45**, 415 (1971).
[28]M. V. Fischetti and S. E. Laux, J. Appl. Phys. **80**, 2234 (1996).
[29]J. Singh, *Physics of Semiconductors and Their Heterostructures* (McGraw-Hill, New York, 1993).
[30]M. V. Fischetti and S. E. Laux, Phys. Rev. B **48**, 2244 (1993).
[31]B. R. Nag, *Electron Transport in Compound Semiconductors*, Springer Series in Solid-State Sciences Vol. 11 (Springer-Verlag, Berlin, 1980).
[32]A. Rahman, M. S. Lundstrom, and A. W. Ghosh, J. Appl. Phys. **97**(5), 053702 (2005).
[33]C. B. Vining, J. Appl. Phys. **69**, 331 (1991).
[34]H. Zhao, Z. Tang, G. Li, and N. R. Aluru, J. Appl. Phys. **99**(6), 064314 (2006).
[35]G. Chen, Phys. Rev. B **57**(23), 14958 (1998).
[36]G. A. Slack, Solid State Phys. **34**, 1 (1979).
[37]G. Chen, J. Heat Transfer **119**(2), 220 (1997).
[38]J. P. Dismukes, L. Ekstrom, E. F. Steigmeier, I. Kudman, and D. S. Beers, J. Appl. Phys. **35**(10), 2899 (1964).
[39]M. Wagner, "Simulation of thermoelectric devices," Ph.D. dissertation, Vienna University of Technology, 2007.